



Calhoun: The NPS Institutional Archive

Faculty and Researcher Publications

Faculty and Researcher Publications

2008

Balanced boundary layers used in hurricane models

Smith, R. K.

Balanced boundary layers used in hurricane models, Q. J. R. Meteorol. Soc., 134, pp. 1385-1395: 2008, Smith, R. K. and M. T. Montgomery



Calhoun is a project of the Dudley Knox Library at NPS, furthering the precepts and goals of open government and government transparency. All information contained herein has been approved for release by the NPS Public Affairs Officer.

Dudley Knox Library / Naval Postgraduate School
411 Dyer Road / 1 University Circle
Monterey, California USA 93943

<http://www.nps.edu/library>

Balanced boundary layers used in hurricane models

Roger K. Smith^{a,*} and Michael T. Montgomery^{b,c,†}

^a *Meteorological Institute, University of Munich, Munich, Germany*

^b *Department of Meteorology, Naval Postgraduate School, Monterey, California, USA*

^c *NOAA Hurricane Research Division, Miami, Florida, USA*

ABSTRACT: We examine the formulation and accuracy of various approximations made in representing the boundary layer in simple axisymmetric hurricane models, especially those that assume *strict* gradient wind balance in the radial direction. Approximate solutions for a steady axisymmetric slab boundary-layer model are compared with a full model solution. It is shown that the approximate solutions are generally poor in the inner core region of the vortex, where the radial advection term in the radial momentum equation is important and cannot be neglected. These results affirm some prior work and have implications for a range of theoretical studies of hurricane dynamics, including theories of potential intensity, that employ balanced boundary-layer formulations. Copyright © 2008 Royal Meteorological Society

KEY WORDS tropical cyclone; typhoon; friction layer; gradient wind balance

Received 30 January 2008; Revised 12 June 2008; Accepted 26 June 2008

1. Introduction

The boundary layer of a mature hurricane has been long recognized as an important feature of the storm. In particular, it controls the radial distribution of moisture, vertical motion and absolute angular momentum that ascends into the eyewall clouds. Early attempts to isolate the dynamics of the boundary layer of a mature hurricane were made by Rosenthal (1962), Smith (1968), Carrier (1971) and Eliassen (1971). These studies highlighted a feature already well known from other areas of fluid dynamics that the boundary layer induces a secondary (overturning) circulation in the vortex above and that this circulation is associated with the imbalance of forces in the layer brought about by surface friction (e.g. Greenspan, 1968). A scale analysis of the boundary-layer equations shows that the vertical gradient of perturbation pressure can be neglected to a first approximation so that the radial pressure gradient in the boundary layer is equal to that in the flow above the layer (Smith, 1968). However, surface friction reduces the tangential wind speed and hence the centrifugal and Coriolis forces in the layer, leaving for a cyclonic vortex a net inward residual force. It is this net force that drives inflow in the layer, thereby inducing a secondary circulation in the vortex itself. Consistent with mass continuity, there is induced subsidence at outer radii and induced ascent at inner radii. In a hurricane, the inflowing air acquires moisture through

evaporation at the sea surface and the moist air ascends to feed the eyewall clouds.

Despite that fact that the induced flow in the boundary layer is associated with gradient wind imbalance in the layer, many representations of the hurricane boundary layer have taken the tangential flow there to be in strict gradient wind balance, but have included a sink of absolute angular momentum at the surface (Ogura, 1964; Ooyama, 1969; Schubert and Hack, 1983; Emanuel, 1986, 1989, 1995, 1997, 2004; Frisius, 2005, 2006; Wirth and Dunkerton, 2006). We are unaware of any reasoned justification for such a formulation, but one could imagine that the dynamics of the balanced boundary layer is essentially different from that in which friction plays an active role, since any inflow in these balance models cannot be ‘driven’ directly by frictional imbalance. At best they may be expected to be a valid first approximation only where the radial flow is sufficiently slow. A natural question then arises, how severe are their limitations? We have shown recently (Smith *et al.*, 2008) that the assumption of balance is poor in Emanuel’s steady-state hurricane model (Emanuel, 1986) and by implication in his theory for potential intensity (Emanuel, 1995; Bister and Emanuel, 1998).

Two of the early pioneering models of hurricanes, those of Ooyama (1969) and Sundqvist (1970), were balanced in the sense that the tangential, or primary, circulation was taken to be in axisymmetric gradient wind balance, and both models were considered to produce reasonably realistic simulations of hurricanes. Indeed, the axisymmetric gradient balance assumption is thought to be a relatively accurate one over most of the free troposphere, except in the upper-level outflow layer, and the assumption is supported by an elementary

*Correspondence to: Roger K. Smith, Meteorological Institute, University of Munich, Theresienstr. 37, 80333 Munich, Germany. E-mail: roger.smith@lmu.de

†The contribution of Michael T. Montgomery to this article was prepared as part of his official duties as a United States Federal Government employee.

scale analysis for a rapidly rotating vortex in which the radial component of flow is much less than the tangential component (Willoughby, 1979). It is supported also by aircraft reconnaissance measurements in the lower troposphere (Willoughby, 1977, 1990). However, these early models assumed that the boundary layer is in gradient wind balance also. Ooyama was aware of the limitations of the latter assumption and wrote in an unpublished manuscript in 1968 ‘... it appears that the weakest hypothesis in the original model is the use of the balance approximation in the boundary layer’. In the manuscript, Ooyama went on to show that solutions with a more complete boundary-layer formulation were more realistic than those with a balanced boundary-layer formulation. As far as we are aware, most authors have not seriously questioned the accuracy of the balanced assumption in the hurricane boundary layer, even though some prior analyses of the layer (Smith, 1968; Carrier, 1971) showed that it is unlikely to be an accurate approximation in the inner core, a finding supported also by more recent numerical simulations of hurricanes (Persing and Montgomery, 2003, Appendix; Kepert and Wang, 2001).

In this paper we revisit this important problem. We present first a novel scale analysis that helps identify a baseline of rational approximations to the steady depth-averaged swirling boundary layer. Then we compare the predictions of various approximate formulations of the boundary layer in a steady slab model, including those that assume gradient wind balance, with that of the unapproximated formulation. Using the unapproximated solution as a benchmark, the accuracy of the various approximate formulations is assessed.

We begin by reviewing the features of balanced models in general, highlighting the role of friction in the secondary circulation as described by the Sawyer–Eliassen equation.

2. Balanced hurricane models

The cornerstone of all balance theories for vortex evolution is the Sawyer–Eliassen (SE) balance model which describes the slow evolution of an axisymmetric vortex forced by heat and (azimuthal) momentum sources. Here the flow is assumed to be axisymmetric and in strict gradient wind and hydrostatic balance. We summarize the SE model here for the simplest configuration, namely the axisymmetric flow of an incompressible Boussinesq fluid with constant ambient Brunt–Väisälä frequency, N . The hydrostatic primitive equations of motion may be expressed in cylindrical polar coordinates (r, λ, z) as

$$\frac{\partial u}{\partial t} + u \frac{\partial u}{\partial r} + w \frac{\partial u}{\partial z} - C = -\frac{\partial P}{\partial r} + F_r, \quad (1)$$

$$\frac{\partial v}{\partial t} + u \frac{\partial v}{\partial r} + w \frac{\partial v}{\partial z} + \frac{uv}{r} + fu = F_\lambda, \quad (2)$$

$$0 = \frac{\partial P}{\partial z} + b, \quad (3)$$

$$\frac{\partial b}{\partial t} + u \frac{\partial b}{\partial r} + w \frac{\partial b}{\partial z} + N^2 w = \dot{B}, \quad (4)$$

$$\frac{\partial ru}{\partial r} + \frac{\partial rw}{\partial z} = 0, \quad (5)$$

where r, λ, z are the radial, azimuthal and vertical coordinates, respectively, (u, v, w) is the velocity vector in this coordinate system, $C = v^2/r + fv$ is the sum of the centrifugal and Coriolis terms, f is the Coriolis parameter, $P = p/\bar{\rho}$ is the pressure p divided by the mean density $\bar{\rho}$ at height z , b is the buoyancy force per unit mass, defined as $-g\{\rho - \bar{\rho}(z)\}/\rho^*$, p is the density, ρ^* is the average density over the whole domain, \dot{B} is the diabatic source of buoyancy, and F_r and F_λ are the radial and tangential components of frictional stress, respectively.

With the additional assumption of gradient wind balance, Equation (1) reduces to

$$C = \frac{\partial P}{\partial r}. \quad (6)$$

If P is eliminated by cross-differentiation with the hydrostatic Equation (3), we obtain the thermal wind equation

$$\frac{\partial b}{\partial r} = \xi \frac{\partial v}{\partial z}, \quad (7)$$

where $\xi = 2v/r + f$ is twice the absolute angular velocity at radius r . The SE equation is obtained by differentiating (7) with respect to time, eliminating the time derivatives of v and b using (2) and (4) and introducing a streamfunction ψ for the secondary circulation such that the continuity equation (5) is satisfied, i.e. we write $u = -(1/r)(\partial\psi/\partial z)$ and $w = (1/r)(\partial\psi/\partial r)$. Then, with a little algebra we obtain

$$\begin{aligned} \frac{\partial}{\partial r} \left\{ \left(N^2 + \frac{\partial b}{\partial z} \right) \frac{1}{r} \frac{\partial \psi}{\partial r} - \frac{S\xi}{r} \frac{\partial \psi}{\partial z} \right\} \\ + \frac{\partial}{\partial z} \left\{ \frac{\xi \zeta_a}{r} \frac{\partial \psi}{\partial z} - \frac{\xi S}{r} \frac{\partial \psi}{\partial r} \right\} = \frac{\partial \dot{B}}{\partial r} - \frac{\partial}{\partial z} (\xi F_\lambda), \end{aligned} \quad (8)$$

where $S = \partial v/\partial z$ is the vertical shear of the tangential wind component and $\zeta_a = (1/r)(\partial rv/\partial r) + f$ is the absolute vertical vorticity. More general derivations of this equation are found, for example, in Willoughby (1979), Shapiro and Willoughby (1982) and Smith *et al.* (2005). The SE equation is elliptic if the vortex is symmetrically stable (i.e. if the inertial stability on isentropic surfaces is greater than zero). It is readily shown that symmetric stability is assured when

$$\left(N^2 + \frac{\partial b}{\partial z} \right) \zeta_a \xi - (\xi S)^2 > 0$$

(Shapiro and Montgomery, 1993). Given suitable boundary conditions, Equation (8) may be solved for the streamfunction of the secondary circulation ψ at a given time. Being a balance model, only one prognostic equation is

used to advance the system forward in time. The set of equations (2) (or (4)), (7) and (8) thus provide a system that can be solved for the balanced evolution of the vortex. Equation (2) (or (4)) along with the diagnostic equation (7) is used to predict the future state of the primary circulation with values of u and w at a given time being computed from the streamfunction ψ obtained by solving (8). The secondary circulation given by (8) is just that required to keep the primary circulation in hydrostatic and gradient wind balance in the presence of the processes trying to drive it out of balance. These processes are represented by the radial gradient of the rate of buoyancy generation and the vertical gradient of ξ times the tangential component of frictional stress. It follows that surface friction can induce radial motion in a balanced formulation of the boundary layer.

The SE equation can be simplified by using potential radius coordinates in which the radius r is replaced by the potential radius, R , defined by

$$\frac{1}{2}fR^2 = rv + \frac{1}{2}fr^2,$$

the right-hand side being the absolute angular momentum (Schubert and Hack, 1983). In this case, surfaces of absolute angular momentum are vertical and the assumption that these surfaces are coincident with the moist isentropes provides an elegant way to formulate the zero-order effects of moist convection (Emanuel, 1986, 1989, 1995, 1997). It is for this reason, perhaps, that balanced models remain popular. Nevertheless, the question remains whether the boundary layer in such models is sufficiently accurate? We explore this question below in the context of a simple slab formulation for the boundary layer and approximations thereto.

3. A slab model for the boundary layer

We review first the slab boundary-layer model described by Smith and Vogl (2008; henceforth SV08), which provides a suitable framework to examine the accuracy of various approximations in boundary-layer formulations. For simplicity we assume first the boundary layer to have uniform depth, h , and constant density as in Emanuel (1986). In our cylindrical coordinate system, the vertically integrated equations for the radial momentum, azimuthal momentum and mass continuity can be written in the following form:

$$u_b \frac{du_b}{dr} = \frac{w_{h-} + w_{sc}}{h} u_b - \frac{(v_g^2 - v_b^2)}{r} - f(v_g - v_b) - \frac{C_D}{h} (u_b^2 + v_b^2)^{1/2} u_b, \quad (9)$$

$$u_b \frac{dv_b}{dr} = \frac{w_{h-} + w_{sc}}{h} (v_b - v_g) - \left(\frac{v_b}{r} + f\right) u_b - \frac{C_D}{h} (u_b^2 + v_b^2)^{1/2} v_b, \quad (10)$$

$$\frac{du_b}{dr} = -\frac{u_b}{r} - \frac{w_h}{h}, \quad (11)$$

where u_b and v_b are the vertically-averaged radial and azimuthal components of wind speed in the boundary layer, $v_g(r)$ and w_h are the tangential wind speed and vertical velocity at the top of the boundary layer, C_D is the surface drag coefficient and $w_{h-} = (w_h - |w_h|)/2$. The terms involving w_{sc} represent turbulent fluxes at the top of the boundary layer (arising from rainbands, shallow convection, or smaller-scale turbulent structures), but for simplicity we do not consider them here, setting w_{sc} equal to zero. Consistent with the slab formulation, the quantities u_b and v_b are assumed to be independent of depth. Note that w_{h-} is non-zero only when $w_h < 0$, in which case it is equal to w_h . Thus the terms involving w_{h-} represent the transport of properties from above the boundary layer that may be different from those inside the boundary layer. As in SV08, we take $C_D = C_{D0} + C_{D1}|u_b|$, where $C_{D0} = 0.7 \times 10^{-3}$ and $C_{D1} = 6.5 \times 10^{-5}$ for wind speeds less than 20 m s^{-1} and $C_D = 2.0 \times 10^{-3}$, a constant, for larger wind speeds. These values are based on our interpretation of Figure 5 from Black *et al.* (2007).

Substitution of (11) into (9) gives an expression for w_h :

$$w_h = \frac{h}{1 + \alpha} \times \left[\frac{1}{u_b} \left(\frac{v_g^2 - v_b^2}{r} + f(v_g - v_b) + \frac{C_D}{h} (u_b^2 + v_b^2)^{1/2} u_b \right) - \frac{u_b}{r} \right], \quad (12)$$

where α is zero if the expression in square brackets is positive and unity if it is negative. With this expression for w_h , (9), (10) and (12) form a system of ordinary differential equations that may be integrated radially inwards from some large radius R to determine u_b and v_b as functions of r , given values of these quantities at $r = R$ as well as the radial profile $v_g(r)$.

In the following subsection we examine several approximations to the foregoing equations.

3.1. Scale analysis

At this stage it is instructive to carry out a scale analysis of (9)–(11). (Whereas some of the criteria to be developed are implicit in the modified Oseen approximation method developed by Carrier (1971) for swirling flow boundary layers with vertical structure, the scale analysis and interpretations herein are believed new.) For simplicity we consider the case where $w_{sc} = 0$. First we set $v_b = v_g + v'_b$ and rewrite the two momentum equations in the form given in Table I. There we have defined

$$\zeta_{ag} = \frac{dv_g}{dr} + \frac{v_g}{r} + f$$

to be the absolute vorticity and $\xi_g = 2v_g/r + f$ to be twice the absolute angular velocity of the gradient wind profile above the boundary layer. We introduce scales U, V, W for (u_b, v_g, w_{h-}) , R, H for the radius r and boundary-layer depth h , V' for v'_b , Λ for ζ_{ag} , and Ξ for ξ_g . The two terms in the continuity equation (11) have scales U/R and W/H , respectively, and

Table I. Scaling of the terms in Equations (9) and (10); see text for details.

Terms in (9)	$u_b \frac{du_b}{dr} =$	$\frac{w_{h-} u_b}{h}$	$+\frac{v_b'^2}{r}$	$+\xi_g v_b'$	$-\frac{C_D}{h} v_b u_b$	(9a)
	$\frac{U^2}{R}$	$\frac{U^2}{R}$	$\frac{V'^2}{R}$	$\Xi V'$	$\frac{C_D}{H} VU$	(9b)
	S_u	S_u	$Ro_{v'}^*$	1	$F_u \frac{U}{V'}$	(9c)
Terms in (10)	$u_b \frac{\partial v'}{\partial r} =$	$\frac{w_{h-} v_b'}{h}$	$-\frac{u_b v_b'}{r}$	$-\zeta_{ag} u_b$	$-\frac{C_D}{h} v_b (v_g + v_b')$	(10a)
	$U \frac{V'}{R}$	$W \frac{V'}{H}$	$\frac{UV'}{R}$	ΛU	$\frac{C_D}{H} V(V + V')$	(10b)
	$Ro_{v'}$	$Ro_{v'}$	$Ro_{v'}$	1	$F_v \frac{V}{U} \quad F_v \frac{V'}{U}$	(10c)

$$Ro_{v'} = V'/(R\Lambda), Ro_{v'}^* = V'/(R\Xi), S_u = Ro_{v'}^*(U/V')^2, F_u = C_D V/(H\Xi) \text{ and } F_v = C_D V/(H\Lambda).$$

since these terms have equal magnitudes, it follows that $W/H \sim U/R$. We use this result in scaling the two terms involving w_{h-} in (9) and (10); see (9a) and (10a) in the table. The scales of each term in these two equations are given in the first row below each equation: (9b) and (10b). These scales are made non-dimensional in the second row below each equation: rows (9c) and (10c). Five non-dimensional quantities arise in this analysis:

- $Ro_{v'} = V'/(R\Lambda)$, a local Rossby number in the tangential momentum equation based on the departure of the tangential wind from the gradient wind (V') and the local absolute vertical vorticity of the gradient wind above the boundary layer (Λ);
- $Ro_{v'}^* = V'/(R\Xi)$, a local Rossby number in the radial momentum equation, again based on V' , but as well on twice the absolute rotation rate (based on the gradient wind) instead of Λ ;
- $S_u = U^2/(R\Xi V') = Ro_{v'}^*(U/V')^2$, a local Rossby number multiplied by the square of the ratio of agradient winds, $(U/V')^2$;
- $F_u = C_D V/(H\Xi)$ and $F_v = C_D V/(H\Lambda)$, non-dimensional forms of the friction terms. These are bulk-aerodynamic Ekman numbers depending on either twice the absolute rotation rate or absolute vorticity, respectively.

Note that $(U/V')^2$, which arises in the expression for S_u , is not necessarily small and might be larger than unity.

3.2. Weak friction approximation

Since the reduction of the tangential wind component in the boundary layer increases with the strength of the frictional force, it is of interest to examine first the case of weak friction, for which $|v_b'| \ll v_g$. This case corresponds to the scaling in which $V'/V \ll 1$. It follows immediately from row (10c) in Table I that

$$\frac{U}{V} \sim F_v. \tag{13}$$

Equation (9a) shows that even in the case of weak friction, the net radial acceleration $-\xi_g v_b'$ will be unopposed unless it is balanced by the radial component of the frictional force. Such a balance would imply that $V'/V \sim F_u(U/V)$, or

$$\frac{V'}{V} \sim F_u F_v. \tag{14}$$

Clearly, for the approximation to be self-consistent, the quantity on the right-hand side of (14) must be much less than unity. The advective part of the radial acceleration in (9a) will be negligible locally only if $S_u \ll 1$, requiring that

$$\frac{U^2}{V^2} \ll \frac{1}{Ro_{v'}^*} \frac{V'^2}{V^2} \tag{15}$$

where V'/V is obtained from (14). Using (13) to estimate U/V , it follows readily that (15) is equivalent to the condition that the local Rossby number

$$Ro_{\Lambda} = \frac{V}{\Lambda R} \ll 1. \tag{16}$$

As shown below, this condition is generally not satisfied in the high wind region of the vortex core and is a valid approximation only at large radii. The stringency of the condition (15), or equivalently (16), will become apparent in section 4. The second term on the right-hand side of (9b) can be neglected if $Ro_{v'}^* \ll 1$, i.e. if $V'/V \ll Ro_{\Xi}$, which we define as $V/(\Xi R)$. In the high wind speed region of the vortex, this local Rossby number is about 1/2. Thus in this region, the neglect of the perturbation centripetal acceleration is justified if $V'/V \ll 1/2$.

With the foregoing scaling assumptions, (10a) approximates to give

$$u_b = -\mu v_g, \tag{17}$$

where

$$\mu = \frac{C_D v_g}{h \zeta_{ag}}. \tag{18}$$

Note that the total wind in the boundary layer, $|v_b|$, can be approximated as v_g to lowest order in U/V and V'/V . At this level of approximation, (9) gives

$$v'_b = v_b - v_g = -v^2 v_g, \tag{19}$$

where

$$v = \frac{C_D v_g}{hI}, \tag{20}$$

and $I^2 = \xi_g \zeta_{ag}$ is the inertial stability parameter. Clearly the integrity of the approximations leading to (17) and (19) depends on both the parameters μ and v^2 being small compared with unity, consistent with (15). The size of these parameters may be readily checked for a given radial profile of the gradient wind, v_g .

3.3. Semi-linear approximation

A common simplification of the full boundary-layer equations is to neglect the terms involving the vertical advection through the top of the layer and to linearize the acceleration terms (Eliassen and Lystad, 1977; Kepert, 2001). If we make such approximations in (9) and (10), again treating the magnitudes of u_b and v'_b as small compared with v_g , but not linearizing the friction term, the equations become

$$\xi(v_g - v_b) = -\frac{C_D}{h}(u_b^2 + v_b^2)^{1/2} u_b, \tag{21}$$

$$\zeta_a u_b = -\frac{C_D}{h}(u_b^2 + v_b^2)^{1/2} v_b. \tag{22}$$

Again, these equations may be solved locally for u_b and v_b in terms of v_g , ξ and ζ_a . Dividing (21) by (22) gives

$$\frac{(v_g - v_b)}{u_b} = \sigma^2 \frac{u_b}{v_b}, \tag{23}$$

where $\sigma^2 = \zeta_{ag}/\xi_g$. It is convenient to write $(u_b, v_b) = v_g(\sigma u, v)$ so that after a little rearrangement, (23) gives the equation for a circle in the (u, v) plane:

$$u^2 + \left(v - \frac{1}{2}\right)^2 = \frac{1}{4}. \tag{24}$$

Squaring (22) and re-arranging gives a second equation relating u and v :

$$\mu^2 v^4 + \mu^2 \sigma^2 u^2 v^2 - \sigma^2 u^2 = 0, \tag{25}$$

which may be solved v^2 to give

$$v = +\sigma \left(\left\{ \frac{1}{4} u^4 + \frac{u^2}{v^2} \right\}^{1/2} - \frac{1}{2} u^2 \right)^{1/2}. \tag{26}$$

noting that $\sigma^2 \mu^2 = v^2$.

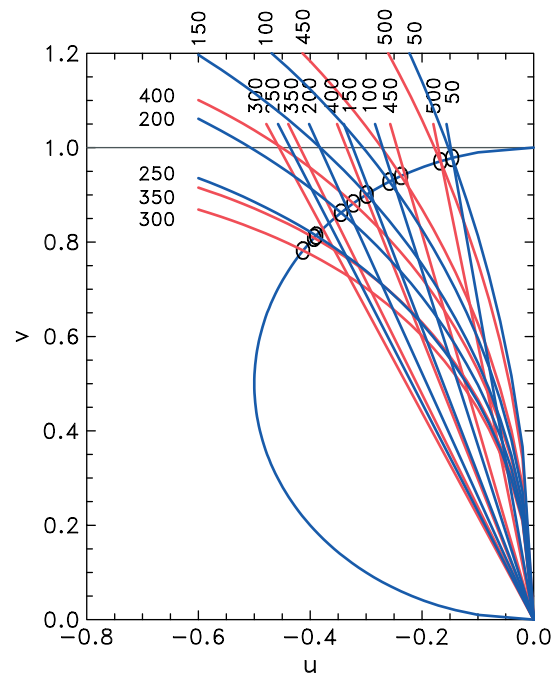


Figure 1. The circle corresponding with Equation (24) and the curves given by Equation (26) for typical values of the parameters σ and v . These parameters are derived from the radial profile of v_g used to construct Figure 2. The straight lines are those given by Equation (27) for the same parameters. The numbers marking the curves are the radii (km) at which the parameters σ and v are calculated. The darker (blue) curves correspond to radii ≤ 250 km and the lighter (red) curves for radii ≥ 300 km. This figure is available in colour online at www.interscience.wiley.com/journal/qj

Families of curves given by (24) and (26) for typical values of the parameters σ and v are shown in Figure 1 (see section 4). The intersections of these curves in the region $u < 0, v > 0$ (assuming a cyclonic vortex for v_g) give the required solutions for (u, v) and hence for (u_b, v_b) . These solutions may be readily obtained by a simple Newton–Rapheson algorithm as explained in the appendix to SV08. The fact that all solutions for (u, v) lie on a circle of radius one half implies a bound on the magnitude of the ratios $\sigma u = u_b/v_g$ and $v = v_b/v_g$, which may not exceed $\sigma/2$ and unity, respectively. Therefore the occurrence of supergradient winds is ruled out in these linear depth-averaged formulations, but u_b could exceed v_g if σ is sufficiently large.

3.4. Geostrophic approximation

If in addition to the semi-linear approximation, we make the small Rossby number assumption, ξ_g and ζ_{ag} may both be approximated by f and (21) and (22) become the slab equivalent of the Ekman layer equations with a quadratic drag law. In this case $\sigma = 1$ and $(u_b, v_b) = v_g(u, v)$. Then the circles given by (24) remain circles in the (u_b, v_b) plane. Moreover, v in (26) reduces to $v_g = C_D v_g / (hf)$.

3.5. Linear approximation

Despite the ability to obtain a solution to the approximate equations with the quadratic friction terms intact, one

might argue that a more consistent approximation of the equations would include also a linearization of the friction terms, replacing $(u_b^2 + v_b^2)^{1/2}$ by v_g , but retaining v_b on the right-hand side of (22). In this case, (24) does not change, but (26) is replaced simply by

$$v = -\frac{\sigma}{\mu}u. \quad (27)$$

The straight lines represented by (27) are shown also in Figure 1. The intersection of these lines with the corresponding circle gives the solution for u and v when the quadratic terms in (21) and (22) are linearized. Note that there are moderate differences between the solutions with and without the linearization of the friction terms for most values of the parameters. Now (21) and (22) reduce to

$$\xi(v_g - v_b) = -\frac{C_D v_g}{h}u_b, \quad (28)$$

$$\zeta_a u_b = -\frac{C_D v_g}{h}v_b. \quad (29)$$

These equations can be written as

$$v_b' = \sigma^2 \mu u_b, \quad (30)$$

$$\text{and } u_b = -\mu(v_g + v_b'). \quad (31)$$

They have the solution

$$u_b = -\frac{\mu v_g}{1 + v^2}, \quad (32)$$

$$\text{and } v_b' = -\frac{v^2 v_g}{1 + v^2}, \quad (33)$$

$$\text{giving } v_b = \frac{v_g}{1 + v^2}. \quad (34)$$

According to the scaling analysis in subsection 3.2, the approximation is self-consistent only if $\mu^2 \ll v^2/Ro_{\Xi} \ll 1/Ro_{\Xi}$. Recall that Ro_{Ξ} is of order one-half in the vortex core region, but becomes small at large radius. If $\mu \sim v$, $S_u \sim 1$ and the inertial (advective) terms become important in the radial momentum equation.

3.6. Balanced approximation

If we make the *strict gradient wind balance* approximation as well as the linear approximation, i.e. if we assume that the tangential wind speed in the boundary layer is equal to that above ($v_b = v_g$), then (21) is bypassed and in the semi-linear case (22) gives directly an expression for the radial wind speed, i.e.

$$\zeta_a u_b = -\frac{C_D}{h}(u_b^2 + v_g^2)^{1/2}v_g. \quad (35)$$

Squaring this equation and solving for u_b gives

$$u_b = -\frac{\mu v_g}{(1 - \mu^2)^{1/2}}. \quad (36)$$

The balanced approximation cannot be rigorously justified as a rational approximation using the foregoing scale analysis since it involves setting $v_b' = 0$ in (9a). Then the value of u_b determined by (10a) does not necessarily satisfy the remaining terms in (9a).

3.7. Emanuel's balanced approximation

Emanuel (1986) made the additional assumption that the radial wind component can be neglected when calculating the total wind speed in the friction term. In this case the radial wind speed is given by

$$u_b = -\mu v_g, \quad (37)$$

which is similar to the dimensional form of (27) except that v_b is approximated by v_g . Moreover, it is the same as (17), which is a feature of the weak friction approximation.

4. Some solutions

In this section we assess the accuracy of the linear and balanced approximations made in subsections 3.3, 3.4, 3.5, 3.6 and 3.7 by comparing the solutions of these equation sets with the corresponding solution of the full equations (9), (10) and (12), which we refer to as the benchmark calculation in the various cases discussed. The profile of v_g is the same as that used in SV08, i.e.

$$v_g = v_1 s \exp(-\alpha_1 s) + v_2 s \exp(-\alpha_2 s),$$

where $s = r/r_m$, and r_m the radius at which the tangential wind speed is a maximum and equal to v_m . In the calculations here, v_m and r_m are taken to be 40 m s^{-1} and 40 km , respectively, and the other parameters are chosen to select the width of the profile: specifically $\alpha_1 = 1.4118$, $\alpha_2 = 0.3$, $v_1 = 103.34 \text{ m s}^{-1}$ and $v_2 = 20.0 \text{ m s}^{-1}$. The Coriolis parameter is taken to be $f = 5 \times 10^{-5} \text{ s}^{-1}$. The geostrophic solution is used to initialize the benchmark calculation at a radius of 500 km , where the local Rossby number $v_g(R)/(fR) = 0.24$ is small enough for this solution to be reasonably accurate (here $v_g(R) = 5.88 \text{ m s}^{-1}$).

4.1. Constant-depth boundary layer

The results of the various calculations are summarized in Figure 2 for a boundary layer with a constant depth of 800 m . The figure shows radial profiles of (inward) radial and tangential wind components in the boundary layer and the vertical velocity component at the top of the boundary layer. The latter is calculated analytically from (12) for the benchmark calculation and from the continuity equation (11) for the approximations to it. Figure 2 shows also the profile of tangential wind assumed at the top of the boundary layer (v_g) and the radial variation of the parameters: μ in (17), (18), (32), (36) and (37); v in (19) and (20); σ in (26); and v^2 in (19), (26) and (32)–(34).

The behaviour of all solutions shows an initial increase in v_b and $|u_b|$ with decreasing radius until certain radii, which are different for v_b and $|u_b|$. In the benchmark solution, the tangential wind speed becomes supergradient ($v_b > v_g$) in the inner core region ($r < 69 \text{ km}$) and because of this, the radial flow suffers a rapid deceleration (SV08) and declines to zero at a radius of about 50 km . At

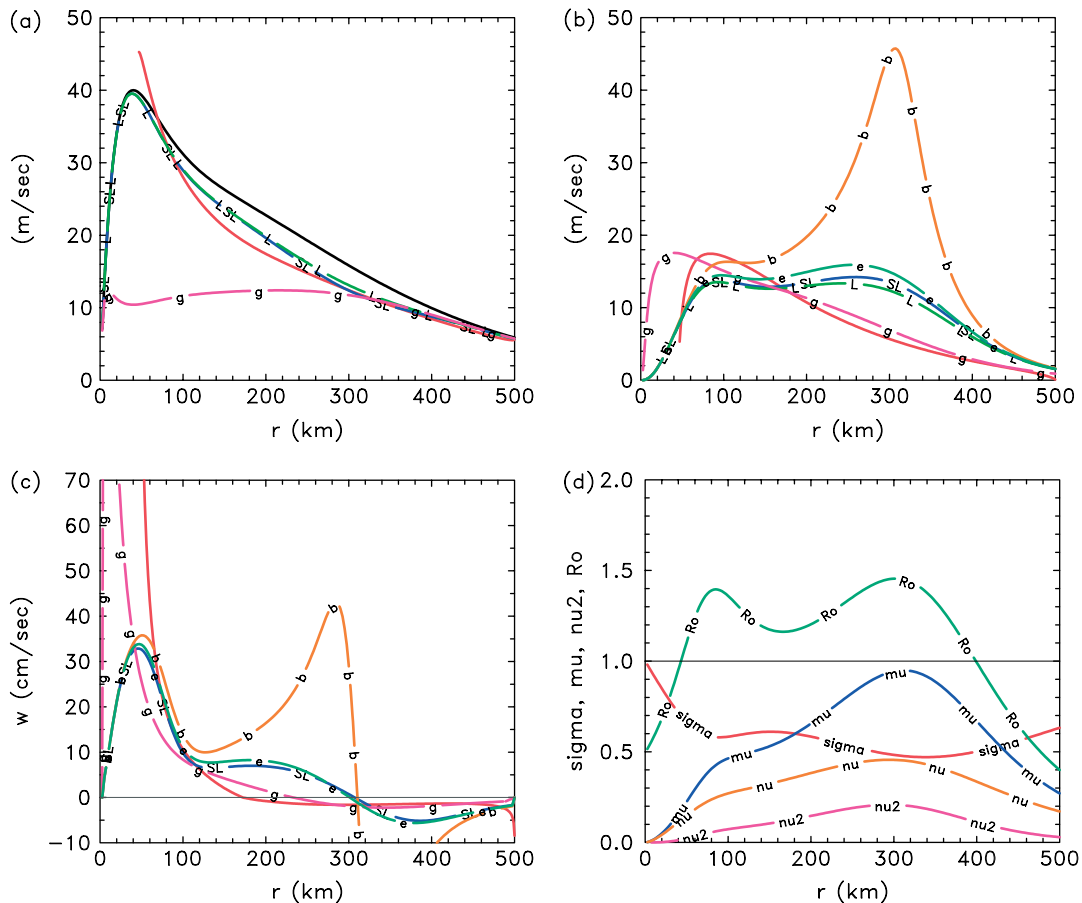


Figure 2. Radial profiles of (a) tangential and (b) radial wind components in the slab boundary-layer calculation described in section 3 and in the various approximations to it. The solid continuous (black) line is the assumed tangential wind profile at the top of the boundary layer, v_g , and those that terminate near a radius of 50 km (red) are the unapproximated boundary-layer solution. Units are $m s^{-1}$. For plotting convenience the sign of u_b has been reversed. ‘SL’ represents the semi-linear solution, ‘L’ the linear solution, ‘g’ the geostrophic solution, ‘b’ the balanced solution and ‘e’ Emanuel’s balanced solution. (c) The corresponding profiles of vertical motion at the top of the boundary layer. (d) The radial variation of the parameters σ , μ , ν , ν^2 and Ro_A (labelled ‘sigma’, ‘mu’, ‘nu’, ‘nu2’, and ‘Ro’, respectively) for the assumed tangential wind profile. This figure is available in colour online at www.interscience.wiley.com/journal/qj

this radius the equations become singular and the solution breaks down. Down to this radius, the tangential wind speed is still increasing inwards. In contrast, in all the approximate solutions, the tangential wind speed remains subgradient, attaining a maximum and then decreasing. None of these solutions become singular. The tangential wind speed in the semi-linear, linear and geostrophic solutions is close to that in the benchmark calculation at radii larger than about 300 km, but the geostrophic solution shows a very large deviation from it at smaller radii. In contrast, the radial wind in the geostrophic calculation follows the benchmark rather closely, except at radii less than 100 km, whereas that in the semi-linear, linear and Emanuel balanced approximations shows a significant deviation from the benchmark at most radii, being a considerable overestimate at radii between about 200 and 400 km and a moderate underestimate at radii around 100 km.

The balance approximation in subsection 3.6 shows an enormous deviation from other solutions, a feature that is attributed to the fact that, at least for the profile chosen for v_g , the parameter μ in (36) approaches unity so that the denominator in (36) becomes relatively

large (Figure 2(d)). Emanuel’s balanced approximation is superior in this respect and the radial wind remains close to the linear solution at all radii, although like the latter, it shows significant departures from the benchmark calculation. There is very little difference between the radial and tangential wind components in the semi-linear and linear calculations.

There are considerable differences in the vertical velocity between the various approximations and the benchmark calculation. The benchmark calculation breaks down at a radius of about 50 km where the radial wind speed tends to zero. This behaviour is not replicated by any of the other solutions. At slightly larger radii, the vertical velocity in the benchmark calculation increases rapidly with decreasing radius, but where there are large radial gradients, the approximations on which boundary-layer theory is based will no longer be valid. Again, the balanced solution shows a large deviation compared with all other solutions between about 200 and 400 km radius. The geostrophic solution predicts large vertical velocities at small radii, while the semi-linear, linear and Emanuel’s balanced solutions show a maximum vertical velocity of about $35 cm s^{-1}$ at a radius of about 60 km.

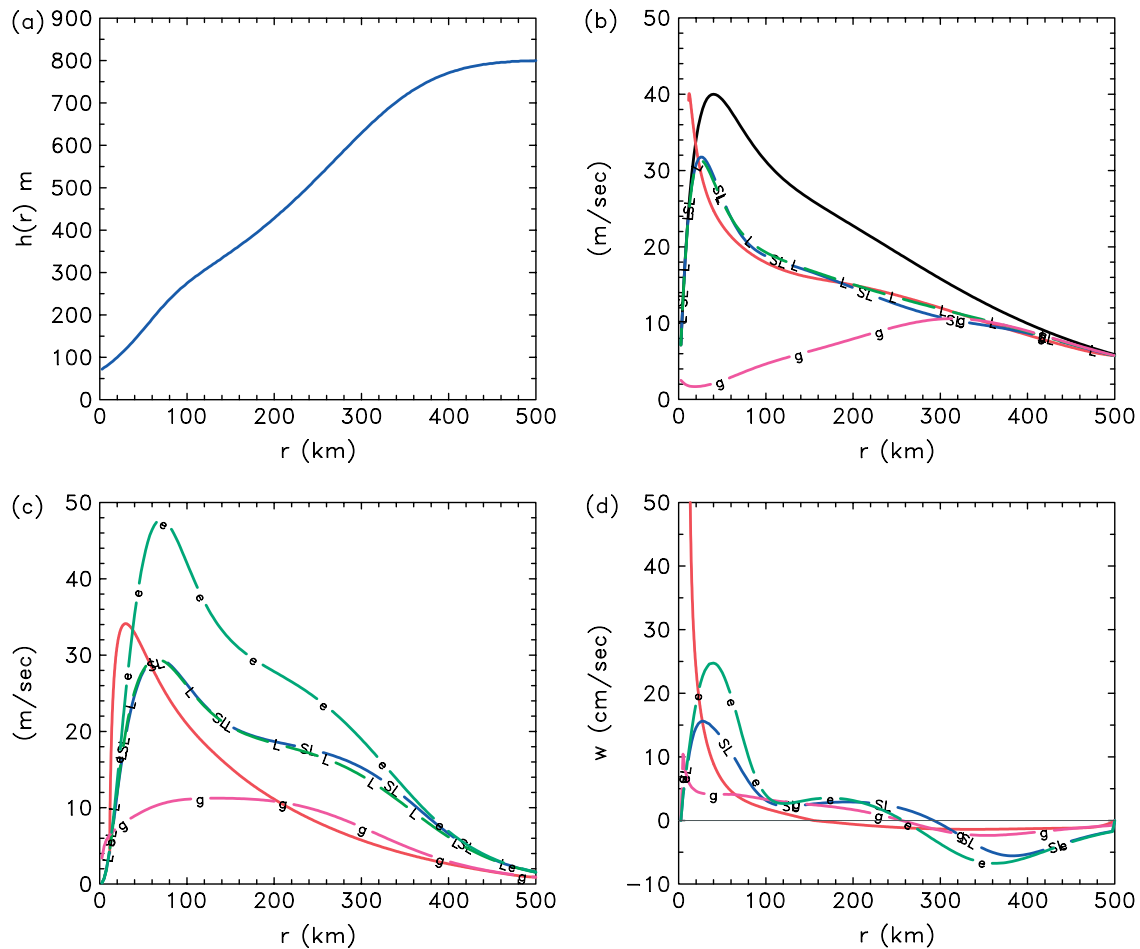


Figure 3. Calculations with variable boundary-layer depth: radial profiles of (a) assumed boundary-layer depth, (b) tangential, and (c) radial wind components in the slab boundary-layer calculation described in section 3 and in the various approximations to it. (d) shows the corresponding profiles of vertical motion at the top of the boundary layer. Lines, labels and units are as Figure 2. This figure is available in colour online at www.interscience.wiley.com/journal/qj

There are significant differences also between the radii at which the vertical velocity changes sign, this being about 170 km in the benchmark calculation, 235 km in the geostrophic calculation, 300 km in Emanuel's balanced calculation and 310 km in the balanced calculation of subsection 3.6. The scale analysis suggests that the poor-ness of the various approximate solutions may be related to the assumption that $Ro_{\Delta} \ll 1$ and $\mu^2 \ll v^2/Ro_{\Sigma} \ll 1/Ro_{\Sigma}$ (section 3.5). Figure 2(d) shows that, at least for the v_g profile chosen, these conditions are far from satisfied.

5. Solutions for radially varying layer depths

A scale analysis of the full boundary-layer equations, without vertical averaging, indicates that the boundary-layer depth is inversely proportional to the square root of the inertial stability, I , at the top of the boundary layer. This scaling would imply a significant reduction in depth between the starting radius and the core region (e.g. Figure 3(a)). Such a variation is supported by the linear solution to the full boundary-layer equations that accounts for vertical structure of the layer (Eliassen and Lystad, 1977; Kepert, 2001) as well as full numerical

solutions (Kepert and Wang, 2001; Montgomery *et al.*, 2001). While it is not possible to determine the radial variation of h in the slab model, it is straightforward to modify (9)–(12) to allow for a prescribed variation $h(r)$ (see SV08, Appendix A). To assess the effect of a decrease in h with declining radius, we carried out calculations in which $h(r) = h(R)\sqrt{I_g/I}$, where $h(R)$ is the boundary layer depth at $r = R$ and I_g is the value of I at this radius. The solutions for $h(R) = 800$ m are shown in Figure 3. In the benchmark calculation the tangential wind speeds in the boundary layer are decreased, especially inside a region of about 200 km and the peak winds are significantly lower in magnitude than v_m . In contrast, the peak radial winds are significantly larger than in the constant-depth calculations and the maximum occurs at markedly smaller radius. When the boundary-layer depth decreases with decreasing radius, the maximum vertical velocity at the top of the layer is reduced considerably from that in the constant-depth calculations and is more in line with that in previous calculations (e.g. Figure 3 of Kepert and Wang, 2001). The variable-depth calculations still show supergradient wind speeds, but now well inside r_m in a region where radial gradients are probably steep enough to strain the

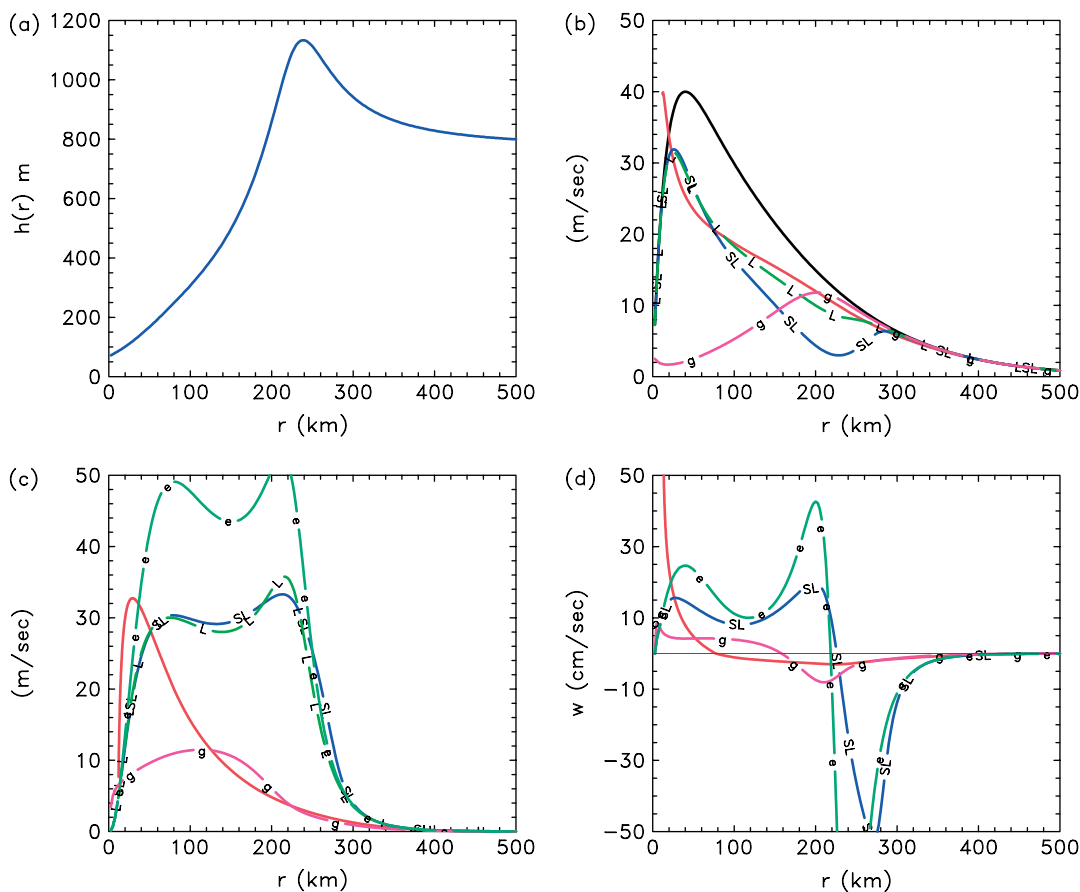


Figure 4. As Figure 3, but for a narrower vortex profile. This figure is available in colour online at www.interscience.wiley.com/journal/qj

assumptions of boundary-layer theory. We have purposely omitted to show the balanced solution of section 3.6 in Figure 3 as the parameter μ^2 in (36) has values larger than unity over a large range of intermediate radii. At these radii, the balanced solution does not exist for the particular v_g profile used.

The semi-linear and linear approximations predict the tangential wind speed rather well, almost up to the radius at which the tangential wind component becomes supergradient in the benchmark calculation. The geostrophic approximation remains accurate inwards to a radius of about 300 km, but greatly underestimates the tangential wind component inside this radius. The predictions of the radial wind component by the approximate theories are all poor in comparison to that in the benchmark calculation except, surprisingly, that of the geostrophic approximation at radii larger than about 200 km. Inside this radius, however, the geostrophic approximation is poor also. The Emanuel balanced approximation and hence the weak friction approximation give by far the worst prediction of the radial component with a maximum exceeding that of the benchmark calculation by 10–20 m s^{-1} at radii between about 70 and 300 km. Note that in these approximations, the radial wind is just minus the ratio of the tangential wind above the boundary layer multiplied by the profile-dependent parameter μ . All the approximate theories overestimate the subsidence into the boundary layer at outer radii (≥ 320 km) and show ascent occurring

inside this radius compared with a radius of 160 km in the benchmark. Moreover the ascent is much larger than in the benchmark except within a radius of about 30 km.

Figure 4 shows plots analogous to those in Figure 3, but for a narrower vortex profile that has the same values of r_m and v_m . (The functional form is the same as before, but $v_1 = 90.06 \text{ m s}^{-1}$, $v_2 = 36 \text{ m s}^{-1}$, $\alpha_1 = 1.601$, $\alpha_2 = 0.5$.) The radius of gale-force winds (17 m s^{-1}) is 317 km compared with 381 km in Figure 3. For this profile, the inertial stability parameter, I , has a local minimum at a radius of about 240 km, which implies a local maximum in the boundary-layer depth at this radius (Figure 4(a)). While this maximum is a natural consequence of the scaling, it is not known how realistic it is because of the lack of observational data on the depth of the inflow layer at these radii in a tropical cyclone. Because the radial gradients are larger, one would expect a narrow vortex profile to strain the balanced approximations more than a broader one and this expectation is confirmed by the solutions. Now the semi-linear balanced approximation is the worst of all of the approximations in capturing the tangential wind component in the boundary layer at radii between 60 and 300 km. In contrast, the semi-linear and linear calculations are reasonably accurate until near the radius at which the tangential wind component in the benchmark calculation becomes supergradient. However the radial wind component is greatly overestimated by all the approximations at a radii less than about 320 km, with

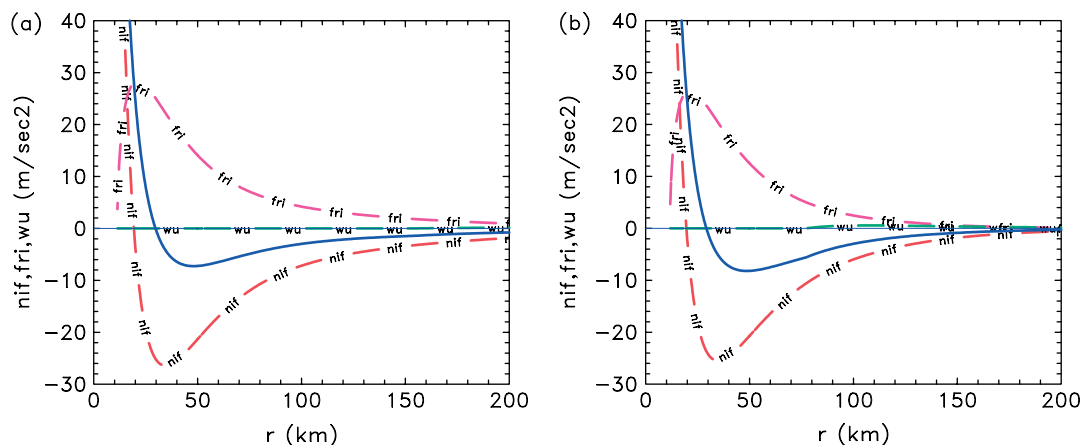


Figure 5. Contributions to the radial momentum balance for radii less than 200 km in the variable-depth calculations in (a) Figure 3, and (b) the narrower vortex profile in Figure 4. The labelling on the curves refers to the net inward force (nif), the frictional force (fri), and the vertical advection of momentum into the boundary layer (wu). The residual force is the solid (blue) line. This figure is available in colour online at www.interscience.wiley.com/journal/qj

the Emanuel balanced calculation being the least accurate. The vertical velocity at the top of the boundary layer is likewise very poor compared with that in the benchmark calculation and worse than in the broader tangential wind profile in Figures 2 and 3.

The reasons for the large deviations of the radial and vertical winds in the balance solutions from those in the benchmark calculation may be inferred from Figure 5, which shows the radial force fields for the two vortex profiles in the calculations with variable boundary-layer depth. The net inward driving force, the difference between the inward pressure gradient force and the outward-directed centrifugal and Coriolis forces, exceeds the frictional force by a significant fraction leaving a net inward force which is just the radial acceleration. This net inward force is appreciable down to the radius just inside r_m , when it begins to decrease rapidly, reversing sign about 10 km outside the radius at which the net driving force changes sign and the tangential wind component becomes supergradient. The foregoing remarks apply to both panels in Figure 5 and, as expected, the radial acceleration is a little larger for the narrower vortex profile.

It is worth pointing out that the benchmark calculation itself is not entirely realistic in these varying-depth calculations. For one thing, the 150 m depth near the radius of maximum gradient wind speed is a factor of two to three too shallow in the inner core region when compared to observations (e.g. Bell and Montgomery, 2008; Kepert, 2006a,b) and for another, the predicted inflow angles, $\tan^{-1}(|u|/v)$, are too large, on the order of 45° , compared with observed maxima of typically $20\text{--}30^\circ$ (e.g. Kepert, 2006a,b). These two shortcomings are presumably related. The shallow depth is a direct consequence of the simple Eliassen and Lystad scaling for a boundary layer with continuous vertical variation assuming a constant eddy diffusivity K and could be addressed by allowing K to increase inwards. Despite these shortcomings, we believe that the results are interesting and worth reporting.

6. Conclusions

Our calculations for the chosen tangential wind profiles v_g show that the semi-linear and linear solutions as well as Emanuel's balanced solution (i.e. the weak friction solution) tend to overestimate the inflow in the boundary layer at large radii (≥ 160 km) and underestimate it at inner radii. In some cases they predict the maximum vertical motion to occur at an unrealistically large radius (>250 km) and they are unable to capture the formation of supergradient winds. The balanced formulation without a linearization of the friction term is especially unrealistic. The inaccuracy of these approximations is suggested by a rational scale analysis of the slab boundary-layer equations since the conditions under which the approximations are derived are not satisfied, at least for the parameters and gradient wind profiles studied here. Therefore, we consider such formulations to be inappropriate for representing the boundary layer in the inner core region of a hurricane.

Acknowledgements

This work was initiated while both authors were visiting the US Hurricane Research Division of NOAA/ AOML. We would like to thank HRD for their hospitality and for creating a stimulating environment for pursuing hurricane research. MTM acknowledges the support of the US Naval Postgraduate School and NSF ATM 0715426.

References

- Bell MM, Montgomery MT. 2008. Observed structure, evolution and potential intensity of category 5 hurricane *Isabel* (2003) from 12 to 14 September. *Mon. Weather Rev.* **136**: 2025–2046.
- Bister M, Emanuel KA. 1998. Dissipative heating and hurricane intensity. *Meteorol. Atmos. Phys.* **65**: 233–240.
- Black PG, D'Asaro EA, Drennan WM, French JR, Niiler PP, Sanford TB, Terrill EJ, Walsh EJ, Zhang JA. 2007. Air–sea exchange in hurricanes: Synthesis of observations from the coupled boundary layer air–sea transfer experiment. *Bull. Am. Meteorol. Soc.* **88**: 357–374.

- Carrier GF. 1971. Swirling flow boundary layers. *J. Fluid Mech.* **49**: 133–144.
- Eliassen A. 1971. On the Ekman layer in a circular vortex. *J. Meteorol. Soc. Japan* **49**: 784–789.
- Eliassen A, Lystadt M. 1977. The Ekman layer of a circular vortex: A numerical and theoretical study. *Geophys. Norveg.* **31**: 1–16.
- Emanuel KA. 1986. An air-sea interaction theory for tropical cyclones. Part I: Steady-state maintenance. *J. Atmos. Sci.* **43**: 585–604.
- Emanuel KA. 1989. The finite-amplitude nature of tropical cyclogenesis. *J. Atmos. Sci.* **46**: 3431–3456.
- Emanuel KA. 1995. Sensitivity of tropical cyclones to surface exchange coefficients and a revised steady-state model incorporating eye dynamics. *J. Atmos. Sci.* **52**: 3969–3976.
- Emanuel KA. 1997. Some aspects of hurricane inner-core dynamics and energetics. *J. Atmos. Sci.* **54**: 1014–1026.
- Emanuel KA. 2004. Tropical cyclone energetics and structure. In *Atmospheric Turbulence and Mesoscale Meteorology*. Fedorovich E, Rotunno R, Stevens B. (eds.) Cambridge University Press: Cambridge, UK.
- Frisius T. 2005. An atmospheric balanced model of an axisymmetric vortex with zero potential vorticity. *Tellus* **57**: 55–64.
- Frisius T. 2006. Surface-flux-induced tropical cyclogenesis within an axisymmetric atmospheric balanced model. *Q. J. R. Meteorol. Soc.* **132**: 2603–2623.
- Greenspan HP. 1968. *Theory of rotating fluids*. Cambridge University Press: Cambridge, UK.
- Kepert JD. 2001. The dynamics of boundary layer jets within the tropical cyclone core. Part I: Linear Theory. *J. Atmos. Sci.* **58**: 2469–2484.
- Kepert JD. 2006a. Observed boundary-layer wind structure and balance in the hurricane core. Part I. Hurricane *Georges*. *J. Atmos. Sci.* **63**: 2169–2193.
- Kepert JD. 2006b. Observed boundary-layer wind structure and balance in the hurricane core. Part II. Hurricane *Mitch*. *J. Atmos. Sci.* **63**: 2194–2211.
- Kepert JD, Wang Y. 2001. The dynamics of boundary-layer jets within the tropical cyclone core. Part II: Nonlinear enhancement. *J. Atmos. Sci.* **58**: 2485–2501.
- Montgomery MT, Snell HD, Yang Z. 2001. Axisymmetric spin-down dynamics of hurricane-like vortices. *J. Atmos. Sci.* **58**: 421–435.
- Ogura Y. 1964. Frictionally controlled, thermally driven circulations in a circular vortex with applications to tropical cyclones. *J. Atmos. Sci.* **21**: 610–621.
- Ooyama KV. 1969. Numerical simulation of the life-cycle of tropical cyclones. *J. Atmos. Sci.* **26**: 3–40.
- Persing J, Montgomery MT. 2003. Hurricane superintensity. *J. Atmos. Sci.* **60**: 2349–2371.
- Rosenthal SL. 1962. 'A theoretical analysis of the field motion in the hurricane boundary layer'. National Hurricane Research Project Report No 56. US Dept of Commerce. Available from NOAA/AOML, Hurricane Research Division, Miami, FL 33149-1026.
- Schubert WH, Hack JJ. 1983. Transformed Eliassen balanced vortex model. *J. Atmos. Sci.* **40**: 1571–1583.
- Shapiro LJ, Montgomery MT. 1993. A three-dimensional balance theory for rapidly rotating vortices. *J. Atmos. Sci.* **50**: 3322–3335.
- Shapiro LJ, Willoughby H. 1982. The response of balanced hurricanes to local sources of heat and momentum. *J. Atmos. Sci.* **39**: 378–394.
- Smith RK. 1968. The surface boundary layer of a hurricane. *Tellus* **20**: 473–483.
- Smith RK, Vogl S. 2008. A simple model of the hurricane boundary layer revisited. *Q. J. R. Meteorol. Soc.* **134**: 337–351.
- Smith RK, Montgomery MT, Zhu H. 2005. Buoyancy in tropical cyclones and other rapidly rotating vortices. *Dyn. Atmos. Oceans* **40**: 189–208.
- Smith RK, Montgomery MT, Vogl S. 2008. A critique of Emanuel's hurricane model and potential intensity theory. *Q. J. R. Meteorol. Soc.* **134**: 551–561.
- Sundqvist HK. 1970. Numerical simulation of the development of a hurricane in a ten-level model. *Tellus* **22**, 359–390.
- Willoughby HE. 1977. Inertia–buoyancy waves in hurricanes. *J. Atmos. Sci.* **34**: 1028–1039.
- Willoughby HE. 1979. Forced secondary circulations in hurricanes. *J. Geophys. Res.* **84**: 3173–3183.
- Willoughby HE. 1990. Gradient balance in tropical cyclones. *J. Atmos. Sci.* **47**: 465–489.
- Wirth V, Dunkerton TJ. 2006. A unified perspective on the dynamics of hurricanes and monsoons. *J. Atmos. Sci.* **63**: 2529–2547.